Atherosclerosis
A finite element study of plaque distribution and stability

Paul Lidgard

2017

LUND
UNIVERSITY

Master's Thesis in Biomedical Engineering

Faculty of Engineering, LTH
Department of Biomedical Engineering

Supervised by
Ingrid Svensson
Magnus Cinthio

Abstract

Atherosclerosis is a chronic disease of arteries. Cardiovascular diseases, of which atherosclerosis is an underlying mechanism, are the most common causes of death globally. The disease is characterised by lipids having penetrated the intima of the artery wall, accompanied by inflammation, fibrosis and endothelial hyperplasia. Accumulated cells, lipids, connective-tissue elements and debris from the blood gives rise to atherosclerotic plaques. These lesions may cause stenosis or rupture, exposing thrombotic materials to the circulatory system.

Two-dimensional finite element simulations of coronary arteries afflicted by atherosclerosis were carried out, with the aim of studying how structural parameters of a lesion affect plaque stability. The Holzapfel-Gasser-Ogden material model was used to model the arterial layers and the plaque excluding the necrotic core, while the hyperelastic neo-Hookean material model covered the necrotic core. Four parameters were studied; plaque circumference, lumen coverage, necrotic core thickness and necrotic core angle. The load was applied as static intraluminal pressure in two steps, first at 80 mmHg and second at 120 mmHg, and the differences in stress distributions between these steps were used as output results. A Tresca stress map over the artery and lesion was created and peak circumferential and Tresca stresses along the plaque-lumen boundary was saved in each simulation.

Results indicate that all parameters considered had an effect on plaque stability, by the increase and/or change in distribution of stresses induced into the lesion. Differences in stress levels due to structural changes in the plaque were in general small when comparing with values available in the literature, but within reason. The most influential parameter on plaque stability was the necrotic core thickness, which directly affects the thickness of the fibrous cap. Changing this parameter gave the largest increase in peak cap stresses of all four parameters, which may be considered significant in terms of plaque stability.

Keywords: Atherosclerosis, Plaque, Stability, Finite element

Preface

This Master's Thesis has been carried out at the Department of Biomedical Engineering at Lund University in collaboration with the Department of Cardiology at Skåne University Hospital.

I wish especially to express my gratitude and appreciation to my supervisor Ingrid Svensson for her guidance and encouragement throughout this project. Without it, I am sure, I would not have come far. I would also like to thank Magnus Cinthio for his help as well as everyone at the Department of Biomedical Engineering, and David Erlinge at the Department of Cardiology.

Finally, I would like to extend many thanks to family and friends, both older and newer from the Master's Thesis group, for supporting me, giving me energy and joy.

Contents

1 Introduction

Atherosclerosis is a chronic disease which causes stenosis in arteries. The atherosclerotic plaque that gives rise to the narrowing of the inner most layer of the artery is an asymmetric composition of cells, connective-tissue elements, lipids and various debris from the blood.[8] Plaques are divided into two main categories; stable and unstable. Unstable plaques generally have higher concentrations of macrophages and foam cells than stable lesions. Furthermore, the extracellular matrix connecting the plaque to the artery wall is weaker in unstable plaques and more prone to rupture.[14]

Atherosclerosis can, if the plaque chronically continues to expand, cause ischemia through a sufficient degree of stenosis. More common, however, is that an unstable plaque ruptures, exposing thrombotic material to the circulatory system. The resulting embolism can obstruct smaller vessels downstream.[15]

The structure of a plaque has been associated with the probability of rupture. Particularly eccentric distributions are more prone to rupture, but the underlying causes for how these structures are formed is less certain. Atherosclerotic plaques arises in specific regions of the arteries, where weak but oscillating shear stresses are present in the endothelial layer. The development of eccentric distributions of plaque is largely determined by local hemodynamic conditions together with the constituents of the artery wall. A better understanding of the pathological processes behind atherosclerosis coupled with shear stress analysis in the endothelial layer could therefore be helpful in the search for regions where unstable plaques are likely to be formed, enabling preventive actions against acute coronary diseases.[21][15]

This project is partly aimed at giving a better understanding of the causes for atherosclerosis, differences between stable and vulnerable plaques and reasons for rupture. The main focus, however, is to study the structural aspects of plaques and how they affect the stability of a lesion. The methodology behind the finite element (FE) simulations can also give an insight into how similar problems can be examined.

1.1 Aim of the thesis

The aim of this project is to answer the following questions:

- What underlying factors causes atherosclerosis? Are there any significant differences between stable and unstable lesions in this regard?
- In what way does the structure of a plaque affect the risk of rupture?
- Can the finite element method be used to give a better understanding of atherosclerosis?

A study of the current understanding of atherosclerosis will be performed, with emphasis on the causes and development. Unstable plaques in particular will be studied together with the environment in which they are formed. A model of a coronary artery inflicted with atherosclerosis will be implemented and simulated with the FE method. Plaque geometry parameters will be changed to enable the evaluation of their respective effect on plaque stability.

2 | Medical Issues

The arterial wall is divided into three regions; the intima, the media and the adventitia, see figure 2.1. In between these layers are the internal and external elastic lamina, which, depending on the type of artery, can either be close to identical to regular elastic laminae (elastic arteries) or appear with a more robust structure (muscular arteries).[7]

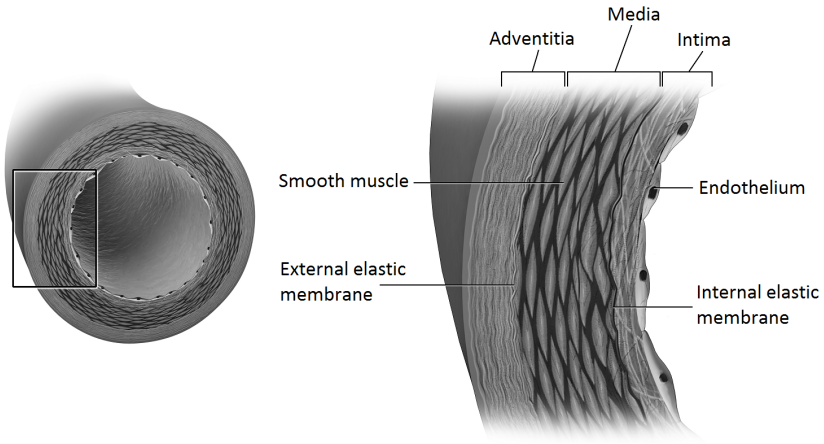

Figure 2.1: Structure of an artery wall. The adventitia, denoted as tunica externa in the figure, is the outermost layer of the wall, followed by the media and intima, with the external and internal elastic membranes between them. The endothelium is a single-cell layer in contact with the lumen. Figure from [3], modified.

2.1 Intima

In young and healthy individuals the intima consists of a single layer of so-called endothelial cells in contact with the blood, hold to the internal elastic membrane by a thin layer of elastin and collagen fibres. Because of its thickness, it only marginally affects the mechanical properties of the wall. The main role of the intima lies instead in the endothelium where chemical substances are produced, aimed at maintaining homeostasis throughout the vessel.[11] These include nitric oxide, endothelin, prostacyclin and angiotensinogen, which hinders platelets, leukocytes and lipoproteins from permeating the vascular wall and works against the formation of blood clots.[15]

Atherscleroses often begins with the entry of lipoproteins and leukocytes into the artery wall. The function of the endothelium is therefore of outmost importance regarding the development of atherosclerotic plaques. The condition of the endothelium is optimal in young and healthy individuals. However, it deteriorates with age, which is associated with thickening of the layer. This thickening is caused by a combination of hypertrophy of the basal membrane and hyperplasia of endothelial cells.[15]

Through arteriosclerosis the intima becomes thicker and stiffens, making the mechanical contribution possibly significant. Regarding atherosclerosis, this effect is local and involves deposition of fatty substances, calcium, collagen fibres, cellular waste products and fibrin.[7]

A secondary subendothelial layer can also be present, varying in size with topography, age and disease. It develops due to non-atherosclerotic intimal thickening and tends to restore baseline stress levels. This layer may contribute to the mechanical properties of the artery wall, depending on its thickness.[7]

2.2 Media

The media forms the bulk of the artery wall and affects the mechanical properties the most.[15] It is the middle layer and consists of a complex structure of smooth muscle cells and elastin and collagen fibres. It is surrounded by the internal and external elastic laminae, which separates it from the intima and adventitia, respectively.[7]

The intermediate layers (the elastin and collagen fibres and the elastic laminae) of the media are closely interconnected, oriented circularly or as a continuous fibrous helix. In between lie smooth muscle cells running mostly circularly but also longitudinally. These layers are well defined and together they form a resilient structure able to resist loads in both the circumferential and the longitudinal direction.[7]

2.3 Adventitia

The outermost layer of an artery wall is called the adventitia and consists mainly of collagen, fibroblasts and fibrocytes. Together with some elastin tissues it merges with the connective tissue that surrounds the artery.[15] The importance of the adventitia is strongly dependent of the type (elastic or muscular) and function of the blood vessel. There is, for instance, more or less no adventitia in cerebral blood vessels.[11]

The collagen is organised in an extracellular matrix, forming two families of helically arranged fibres. However, the deviation from this orientation is large within both families. In load-free conditions the

collagen fibres have a wavy form but straightens at higher levels of pressure. The stiffness of the adventitia thus increases until the fibres are fully straightened, preventing overstretch and rupture of the artery.[7]

2.4 Atherosclerosis

Atherosclerosis is primarily a disease of the intima, characterised by lipids having penetrated the intima accompanied by inflammation, fibrosis and hyperplasia of the endothelium. Problems associated with atherosclerosis are many; it may limit blood flow, serve as a site for embolism, alter the mechanical properties of the wall and weaken it and even impair cardiac function. Furthermore, it may also change endothelial function, vascular tone and cell adhesion to molecules and platelets.[15]

Cardiovascular diseases (CVD), of which atherosclerosis is an underlying mechanism, are the most common cause of death globally. In 2012 alone, an estimated 17.5 million people died from CVDs, or 31 % of all deaths that year. 7.4 million of these were caused by coronary heart disease while 6.7 million were due to stroke.[25]

Behavioural risk factors of CVD include cigarette smoking, unhealthy diet, physical inactivity and harmful use of alcohol. Other risks include hypertension, hypercholesterolemia, diabetes, obesity and old age.[15][25]

Atherogenesis

The known systemic risk factors for atherosclerosis are general and affect the whole circulatory system equally. However, atherosclerotic plaques are formed at specific regions in the system, such as where disturbed blood flows occur (e.g. inner wall of curves and close to bifurcations) causing relatively longer contact between the elements of the blood and the endothelial cells as well as fluctuations in wall stresses.[15] Local hemodynamic forces, including endothelial shear stress (ESS) and blood pressure-derived tensile stress, are important to consider in the localisation of atherosclerosis.[23]

Theories of how atherosclerosis develops at particular sites include incorporation of a thrombus into the vessel wall, local weakening of endothelial function, reaction to injury or a combination of the above.[15] The above mentioned ESS affects the endothelial layer on the cellular level, and differs considerably over short distances in the longitudinal and circumferential directions. Low and oscillatory ESS, ($<$ 1.0 - 1.5 Pa) is associated with atherosclerosis, and is common in side branches, the outer waist of bifurcations and on the inner side of a curve, see figure 2.2. Moderate, physiological ESS is instead unidirectional and in the range of 1.5 - 3.0 Pa.[23] The exact boundaries defining low ESS varies however, both among species and between different arteries.[4]

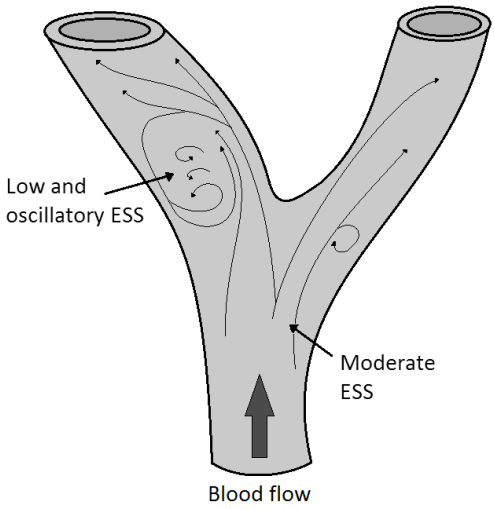

Figure 2.2: Typical location of low and oscillatory ESS, where the probability of plaque development is higher. Magnitude of low time-average ESS is usually less than 1.0 - 1.5 Pa, while moderate, physiological ESS is unidirectional and in the range of 1.5 - 3.0 Pa, although exact intervals vary[23]. Figure recreated from [23].

Endothelial cells uses ESS as stimuli for the expression of certain genes. In regions with moderate levels of ESS, various atheroprotective genes are given a boost, while several atherogenic ones are suppressed. The reverse is true in regions where ESS is low and/or oscillates, thereby promoting the growth of atherosclerotic plaques.[4] These genes includes how the production of nitric oxide and endothelin is regulated, cell shape and the production of reactive oxygen species (for the oxidation of cholesterol). Low ESS also raises endothelial cell apoptosis and causes accumulation of cholesterol into the subendothelial layer.[23] Furthermore, it indirectly promotes permeation of monocytes into the intima, where they evolve through macrophages into foam cells, sustaining the early stages of atherosclerotic lesions.[14]

Inflammation plays a key role in atherogenesis. The early atherosclerotic plaque is dominated by immune cells which, when activated, reduces plaque stability and (in the event of plaque rupture) leads to an acceleration of thrombus development. Lipoproteins that have permeated the endothelium initiates the inflammatory response, and activates the endothelial cells. These in turn then produces molecules adhering to leukocytes (particularly monocytes and lymphocytes), causing the blood cells to gather around the site of inflammation and further promotes production of macrophages.[8]

Plaque Characteristics

Not all atherosclerotic lesions evolve into high-risk plaques prone to rupture. Lesions may also occupy space without affecting the lumen, since the arterial wall is able to adapt by increasing its external radius. With regards to their composition, plaques are heterogeneous. However, stable lesions are usually identified with dense, uniform fibrous caps and are predominantly composed of collagen. Increased vulnerability follows from a reduced amount of smooth muscle cells, an increased amount of macrophages, and a large so-called necrotic core (NC) containing high concentrations of lipids and macrophages.[6] An active inflammation and low ESS not only promotes plaque growth but also promotes the progression of a plaque into a vulnerable type.[18][21]

Figure 2.3 shows an artery narrowed by an atherosclerotic lesion. Smooth muscle cells and macrophages turned into foam cells have accumulated in the endothelial lining along with lipids, minerals and cellular debris, building up the plaque.[22] The variation in plaque composition is large. Lesions may progress to atheromas containing a lipid-laden core, undergo calcification or be rich in collagen fibres with few lipid cells. The mechanical stiffness therefore depends on the type of lesions; calcified and fibrous plaques are much more rigid than cellular ones, and calcified lesions are less associated with plaque rupture.[24]

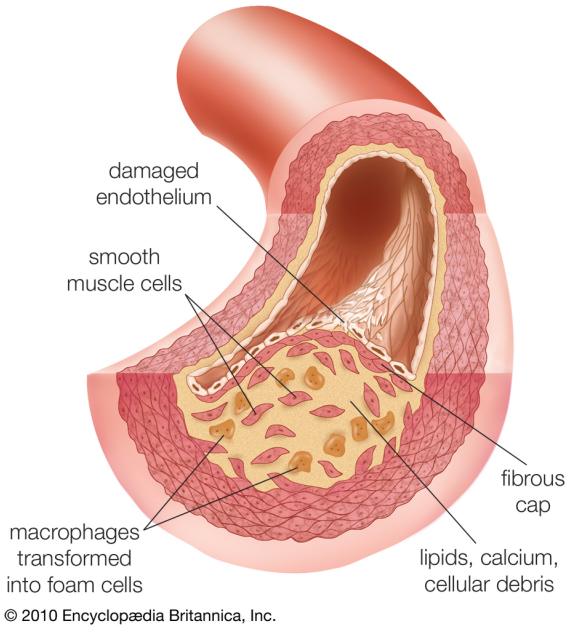

Figure 2.3: Artery narrowed by an atherosclerotic lesion. Image from [22], modified.

3 | Literature survey

This section presents short descriptions of three studies related to this project. All of them attempts to simulate atherosclerosis by means of the finite element method, but with different methodologies and focus.

The aim of this section is to show how the modelling of atherosclerosis problem can be addressed in different ways, and to give an insight into how the results vary between studies. The section does not attempt to fully summarise the respective studies.

3.1 Circumferential stress distribution

The distribution of circumferential stress in diseased coronary arteries is analysed in [5]. Twelve stable control lesions are compared to twelve ruptured ones by the use of finite element models. Prerupture descriptions of the ruptured specimens are available, so that tracings of the cross-sectional geometries of them as well as the stable lesions can be created. The tracings are divided into four regions; artery, fibrous plaque, calcified plaque and lipid pool. The biomechanical behaviour of all components are approximated by linear elastic material parameters, see table 3.1, with the assumption of transverse isotropy for the artery and fibrous plaque.

Table 3.1: Material parameters used in [5]. E_r and E_θ are the Young's moduli in the radial and circumferential directions, $G_{r\theta}$ is the shear modulus and $\nu_{r\theta}$ and $\nu_{\theta z}$ are the Poisson ratios. The parameters for lipid and calcified plaque are $E = 1$ kPa and 10 MPa, respectively, and $\nu = 0.48$ for both.

	E_r (kPa)	E_θ (kPa)	$G_{r\theta}$ (kPa)	$\nu_{r\theta}$	$\nu_{\theta z}$
Artery	10	100	50	0.01	0.27
Plaque	50	1000	500	0.01	0.27

Finite element meshes of all lesions are created based on the geometrical and compositional information from the tracings, with parabolic plane strain elements. After solving for an intraluminal pressure load of 110 mmHg, contour plots of circumferential stresses in the lesions are displayed. Regions in the contour plots with stress values of 300 kPa or higher are identified as regions of high stress, but it is not assumed that all plaques necessarily rupture at this value. Furthermore, in the case

of the ruptured lesions, the locations of the high stress regions in the plaques are compared to the actual site of rupture.

The results show that the group of ruptured lesions has an average peak circumferential stress of 545.4±159.9 kPa, while the control lesions average 192.5±64.7 kPa in peak stress. There are a total of 31 high stress regions in the ruptured lesions with at least one in each, while only a single high stress region is found in all control lesions together. From an approximate lumen centre in each model of ruptured lesions, the angle between highest circumferential stress concentration and rupture location ranges from $-137°$ to $+90°$, with seven of 12 within $15°$ from each other. The angle between nearest high stress region and rupture ranges from $-14°$ to $+37°$, with ten out of 12 within $15°$ from each other.

The study concludes that circumferential tensile stress may play an important role in plaque rupture. It suggests that, since rupture location and highest stress region does not always coincide, variations in local plaque material properties also contribute to fracture.

3.2 Initial stress

In [20], focus is laid on the initial stress (IS) state on the plaque. Fifty two-dimensional finite element models are created from segmented histological sections of diseased coronary arteries, fixed at 100 mmHg. The adventitia is not included in the model and the large part of the plaque excluding the necrotic core is modelled as the intima. The hyperelastic *neo-Hookean* material model (see section 4.2) is used for all segments, with parameters $D = 1e^{-5}$ kPa for all components and $c = 250, 50$ and 5 kPa for the media, intima and necrotic core, respectively.

The intraluminal pressure is in 15 steps increased up to the fixation pressure of 100 mmHg. Stress analysis is performed at each step and the resulting stresses throughout the geometry are applied as initial conditions to the original geometry in the next pressure step. After reaching the initial state, a pressure of 140 mmHg (representing a peak in systole) is applied in 5 steps and stresses and deformations are computed regularly. The results are then compared to corresponding results from straightforward analysis without IS.

The results show differences between using IS and not. Average von Mises stress at the fibrous cap is 92±63 kPa without and 87±56 kPa with IS ($p = 0.09$). The final lumen area also differs between the two cases, from an average increase of 54 % ±14 % without to 18 % ±6 % with IS.

It is concluded that the "general relations between geometrical features and peak cap stress remain intact", and that accounting for IS may improve plaque-specific analyses of rupture risk.

3.3 Three-dimensional analysis

In [17], a three-dimensional finite element model is created based on intravascular ultrasound (IVUS) images. The geometry is reconstructed using 17 cross-sectional images of a lesion located in the right coronary artery, in which the lumen, plaque components (called dense and cellular fibrosis) and media are manually segmented based on the ultrasound attenuation and reflection. A layer of adventitia (with a mean thickness of 350 μm) is then added to the geometry. The segments are modelled as transversally isotropic materials, the parameters can be seen in table 3.2, and partial displacement limitations are imposed to avoid rigid body motion. These limitations are set as zero displacement at the lines where two perpendicular planes intersects with the outer border of the adventitia. The whole of the adventitia's external border is also assumed to be stress-free and the applied load is set as an internal pressure of 100 mmHg.

Table 3.2: Material parameters used in [17]. E_r, E_θ and E_z are the Young's moduli in the radial, circumferential and axial directions, $G_{r\theta}$ is the shear modulus and $\nu_{r\theta}$ and $\nu_{\theta z}$ are the Poisson ratios.

	E_r (kPa)	$E_\theta = E_z$ (kPa)	$G_{r\theta}$ (kPa)	$\nu_{r\theta}$	$\nu_{\theta z}$
Adventitia	80	800	400	0.01	0.27
Media	10	100	50	0.01	0.27
Cellular fibrosis	20	200	100	0.01	0.27
Dense fibrosis	100	1000	500	0.01	0.27

The computed peak circumferential stresses have a mean value of 65.6±21.4 kPa, and are within the range of 33-103 kPa. The location of the highest computed stress is not close by the site of highest stenosis severity, although high-stress regions are found in this region.

The patient from which the images are acquired undergoes balloon angioplasty at the site of the lesion, after which IVUS imaging is performed again. This is done to locate the region of plaque rupture so that the predictability of rupture location from the simulations can be asserted. The study concludes that the model "predicts quite well" the location of rupture, with a concentration line of circumferential stress located in the actual plaque rupture region.

4 | Models and theory

There has been many different attempts at modelling the mechanical behaviour of arterial tissue and plaque components. Linear- or hyperelasticity, isotropy, transverse isotropy, incompressibility, plane strain and pulsatile blood flow are but a few aspects that has been considered (see for instance [11] and [13] or the studies presented in section 3).

The material models to be used are the *Holzapfel-Gasser-Ogden* (HGO) model[7] for the arterial layers and the *neo-Hookean* hyperelastic model (see for example [16]) for the necrotic core. The HGO model is based the non-linear theory of anisotropic elasticity, with the addition of accounting for the dispersion of collagen fibres within the arterial layers. This added complexity requires only one scalar parameter and helps to capture the typical mechanical responses of arterial tissue.

4.1 Constitutive model - Holzapfel-Gasser-Ogden

In the HGO material model, it is assumed that the strain energy potential Ψ, i.e. the energy stored by a system undergoing deformation, can be described by a superposition of an isotropic potential and two transversely isotropic potentials. The isotropic part, Ψ_g, represents the non-collagenous groundmatrix of the arterial layer, while the transversely isotropic parts, Ψ_{fi} $(i = 1, 2)$, represents two embedded families of collagen fibres. The fibres are assumed to be distributed with rotational symmetry about a mean orientation $\boldsymbol{a}_0$ with no radial component, although they are dispersed. The arteries are also assumed to be incompressible.

Assume the existence of an orientation density function $\rho(\boldsymbol{M})$, where $\boldsymbol{M}$ is a three dimensional (Eulerian) unit vector. It is the fibre orientation distribution, and is characterised by the angles $\theta \in [0, \pi]$ and $\phi \in [0, 2\pi]$ (i.e. $\boldsymbol{M}(\theta, \phi)$), see figure 4.1. The normalising condition,

$$\frac{1}{4\pi} \int_\omega \rho(\boldsymbol{M}(\theta, \phi)) \mathrm{d}\omega = 1, \tag{4.1}$$

is assumed to hold, where ω is the unit sphere and $\mathrm{d}\omega = \sin\theta \, \mathrm{d}\theta \mathrm{d}\phi$. With these conditions on ρ defined, the distribution of fibres can be expressed with a second order structural tensor $\boldsymbol{H}$, as

$$\boldsymbol{H} = \frac{1}{4\pi} \int_\omega \rho(\boldsymbol{M}) \boldsymbol{M} \times \boldsymbol{M} \mathrm{d}\omega. \tag{4.2}$$

With the full expression of $\boldsymbol{M}$,

$$\boldsymbol{M}(\theta,\phi) = \sin\theta\cos\phi\,\boldsymbol{e}_1 + \sin\theta\sin\phi\,\boldsymbol{e}_2 + \cos\theta\,\boldsymbol{e}_3, \tag{4.3}$$

it is simpler to see that $\boldsymbol{H}$ can be written in the more compact form

$$\boldsymbol{H} = \sum_{i,j=1}^{3} \alpha_{ij}\boldsymbol{e}_i \times \boldsymbol{e}_j, \tag{4.4}$$

where the coefficients $\alpha_{ij} = \alpha_{ji}$ are

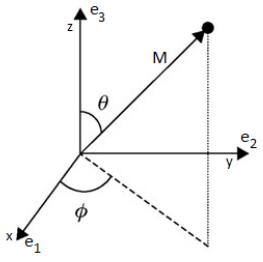

Figure 4.1: Orientation vector $\boldsymbol{M}$ in Eulerian space.

$$\begin{aligned}
\alpha_{11} &= \frac{1}{4\pi}\int_\omega \rho(\boldsymbol{M})\sin^3\theta\cos^2\phi\,\mathrm{d}\theta\mathrm{d}\phi,\\
\alpha_{22} &= \frac{1}{4\pi}\int_\omega \rho(\boldsymbol{M})\sin^3\theta\sin^2\phi\,\mathrm{d}\theta\mathrm{d}\phi,\\
\alpha_{33} &= \frac{1}{4\pi}\int_\omega \rho(\boldsymbol{M})\cos^2\theta\sin\theta\,\mathrm{d}\theta\mathrm{d}\phi,\\
\alpha_{12} &= \frac{1}{4\pi}\int_\omega \rho(\boldsymbol{M})\sin^3\theta\sin\phi\cos\phi\,\mathrm{d}\theta\mathrm{d}\phi,\\
\alpha_{23} &= \frac{1}{4\pi}\int_\omega \rho(\boldsymbol{M})\sin^2\theta\cos\theta\sin\phi\,\mathrm{d}\theta\mathrm{d}\phi,\\
\alpha_{13} &= \frac{1}{4\pi}\int_\omega \rho(\boldsymbol{M})\sin^2\theta\cos\theta\cos\phi\,\mathrm{d}\theta\mathrm{d}\phi.
\end{aligned}$$

If $\boldsymbol{a}_0$ is taken as to align with the basis vector $\boldsymbol{e}_3$, the density function becomes independent of ϕ ($\rho(M(\theta,\phi)) \to \rho(\theta)$), the normalising condition (equation (4.1)) is reduced to

$$\int_0^\pi \rho(\theta)\sin\theta\,\mathrm{d}\theta = 2, \tag{4.5}$$

and the non-diagonal elements of α_{ij} vanish. The remaining elements are given by

$$\alpha_{11} = \alpha_{22} = \kappa,\ \alpha_{33} = 1-2\kappa,\ \kappa = \frac{1}{4\pi}\int_0^\pi \rho(\theta)\sin^3\theta\,\mathrm{d}\theta, \tag{4.6}$$

and the structure tensor $\boldsymbol{H}$ can be rewritten as

$$\boldsymbol{H} = \kappa\boldsymbol{I} + (1-3\kappa)\boldsymbol{\alpha}_0 \times \boldsymbol{\alpha}_0, \tag{4.7}$$

where $\boldsymbol{I}$ is the identity tensor. The introduced parameter κ can be regarded as a structural parameter which represents the fibre distribution, and is obtainable through experimental data.

The distribution of the embedded families of collagen fibres is modelled by a modified version of the π-periodic *von Mises* distribution, with density function

$$f(x|\mu,b) = \frac{e^{b\cos(x-\mu)}}{2\pi I_0(b)}, \quad I_0(\kappa) = \frac{1}{\pi}\int_0^\pi e^{\kappa\cos\Theta}\,\mathrm{d}\Theta. \tag{4.8}$$

I_0 is here the modified *Bessel function* of order 0. Assuming that the fibre distribution is centred around $\theta = 0$, integrating (4.8) according to (4.1) and normalising gives

$$\rho(\theta) = 4\sqrt{\frac{b}{2\pi}}\frac{e^{b(\cos 2\theta+1)}}{-i\frac{2}{\sqrt{\pi}}\int_0^{\sqrt{2b}} e^{-t^2}\mathrm{d}t} = 4\sqrt{\frac{b}{2\pi}}\frac{e^{b(\cos 2\theta+1)}}{\mathrm{erfi}(\sqrt{2b})}, \tag{4.9}$$

where $\mathrm{erfi}(x)$ is the imaginary error function.

As stated, the energy potential $\bar{\Psi}$ is represented by a superposition of an isotropic potential $\bar{\Psi}_\mathrm{g}$ and two transversely isotropic potentials $\bar{\Psi}_{\mathrm{f}i}$. With the use of the structural tensor (4.7), the function becomes

$$\bar{\Psi}(\bar{\boldsymbol{C}}, \boldsymbol{H}_i) = \bar{\Psi}_\mathrm{g}(\bar{\boldsymbol{C}}) + \sum_{i=1,2}\bar{\Psi}_{\mathrm{f}i}(\bar{\boldsymbol{C}}, \boldsymbol{H}_i(\boldsymbol{a}_{0i}, \kappa)) \tag{4.10}$$

where $\bar{\boldsymbol{C}}$ is a modified right Cauchy-Green tensor (see [10] for derivation from the right Cauchy-Green tensor $\boldsymbol{C} = \boldsymbol{F}^\top\boldsymbol{F}$, where $\boldsymbol{F}$ is the deformation gradient tensor). For the transversely isotropic free-energy functions $\bar{\Psi}_{\mathrm{f}i}$, the following form is used:

$$\begin{aligned}&\bar{\Psi}_{\mathrm{f}i}(\bar{\boldsymbol{C}}, \boldsymbol{H}_i) = \frac{k_1}{2k_2}\Big[e^{k_2\bar{E}_i^2} - 1\Big],\\ &i = 1,2, \quad k_1, k_2 > 0, \quad \bar{E}_i = \boldsymbol{H_i} : \bar{\boldsymbol{C}} - 1.\end{aligned} \tag{4.11}$$

$\boldsymbol{H}_i : \bar{\boldsymbol{C}}$ is an invariant of $\boldsymbol{H}_i$ and $\bar{\boldsymbol{C}}$ (see *Frobenius* inner product) and $\bar{E}_i$ represents the strain in the direction of $\boldsymbol{a}_{0i}$. k_1 is a parameter related to stress (deductible from mechanical testing) and k_2 is a dimensionless parameter. Inserting (4.7) into (4.11) and calculating gives

$$\bar{\Psi}_{\mathrm{f}i}(\bar{\boldsymbol{C}}, \boldsymbol{H}_i) = \frac{k_1}{2k_2}\Big[e^{k_2\left(\kappa\bar{I}_1 + (1-3\kappa)\bar{I}_{4i} - 1\right)^2} - 1\Big], \tag{4.12}$$

where $\bar{I}_1 = \mathrm{Tr}\,\bar{\boldsymbol{C}}$ (the first tensor invariant of $\bar{\boldsymbol{C}}$) and $\bar{I}_{4i} = \boldsymbol{a}_{0i}\times\boldsymbol{a}_{0i} : \bar{\boldsymbol{C}}$ (invariant equal to the stretch squared in $\boldsymbol{a}_{0i}$'s direction).

As for the isotropic part of the potential, representing the ground-matrix of the arterial layer, it is represented by an incompressible *neo-Hookean* model,

$$\bar{\Psi}_g = \frac{1}{2}c(\bar{I}_1 - 3), \tag{4.13}$$

where $c > 0$ is a stress-like parameter and $\bar{I}_1$ is again the first tensor invariant of $\bar{\boldsymbol{C}}$.

The finite element software used in the project, Abaqus/CAE (v. 6.14-5), also includes a term for the incompressibility of the material. This is because the program has no mechanism for implementing an incompressibility constraint at each calculation point. The term

$$\frac{1}{D}\Big[\frac{(J^{el})^2-1}{2}-\ln J^{el}\Big], \tag{4.14}$$

where J^{el} is the elastic volume ratio (related to both the total and thermal volume ratio, see [1]), is therefore added to the strain energy potential. Adding all terms together gives the final form of the strain energy potential,

$$\begin{aligned}\bar{\Psi}(\bar{\boldsymbol{C}},\boldsymbol{H}_i) =& \frac{1}{2}c(\bar{I}_1-3)+\frac{1}{D}\Big[\frac{(J^{el})^2-1}{2}-\ln J^{el}\Big] \\ & \frac{k_1}{2k_2}\sum_{i=1,2}\Big[e^{k_2\left(\kappa\bar{I}_1+(1-3\kappa)\bar{I}_{4i}-1\right)^2}-1\Big].\end{aligned} \tag{4.15}$$

4.2 Constitutive model - neo-Hookean

The classical neo-Hookean model is used to model the necrotic core of the atherosclerotic plaque. The model is able to describe non-linear stress-strain responses of a material, and is often used for materials with rubber-like properties. The strain energy potential is given (in the compressible case) by

$$W = c(\bar{I}_1-3)+\frac{1}{D}(J_{el}-1)^2 \tag{4.16}$$

where $c>0$ and D are material constants, $\bar{I}_1$ is the first deviatoric strain invariant of the right Cauchy-Green deformation tensor $\boldsymbol{C}$, i.e.

$$\bar{I}_1 = \bar{\lambda}_1^2+\bar{\lambda}_2^2+\bar{\lambda}_3^2, \tag{4.17}$$

and J^{el} is the elastic volume ratio, see [1]. The deviatoric stretches are given by $\bar{\lambda}_i = J^{-1/3}\lambda_i$, where J is the total volume ratio and λ_i are the principal stretches.

5 | Method

The methodology of the simulations carried out in this project are presented in this section. It will describe how artery segments and plaques were constructed, implementation of the material models, procedure of the simulations and extraction of results.

5.1 Geometry

The issue at hand was simplified by treating it as a two-dimensional problem. As such, the geometry used in the simulations where thought of as cross-sections of an artery afflicted by an atherosclerotic plaque. The structure of this plaque was broken down to four different parameters, which were to be analysed with regards to plaque stability. These parameters were

- Plaque circumference - percentage of arterial wall circumferentially covered by plaque
- Lumen coverage - percentage of original lumen area covered by plaque
- Necrotic core thickness - size of necrotic core radially
- Necrotic core angle - necrotic core spread circumferentially

Each parameter's influence over plaque stability was studied by varying them one at a time.

The complete geometry of the artery wall together with the plaque was created with Matlab, where the position of relevant points (e.g. necrotic core and plaque circumferential ends) were calculated. The parameters used for artery segments sizes were calculated from data and ratios presented in [9], and can be seen in table 5.1.

Table 5.1: Radii of lumen and artery segments, in mm. Each layer's outer radius is presented.

	Lumen	Intima	Media	Adventitia
Radius (mm)	3.6495	3.8791	4.1853	4.5255

While the dimensions of the artery wall segments were fixed and source-based, the plaque geometry parameters were chosen to cover a

broad range of possible distributions. The varying of the parameters were done according to table 5.2, and the relation between each changing parameter and the others is shown in table 5.3. An example of the whole geometry of an artery wall together with a plaque is shown in figure 5.1.

Table 5.2: Plaque structure parameters.

Plaque circumference (%)	Lumen size (%)	NC thickness (mm)	NC angle (°)
55	25	0.5	30
60	30	0.75	45
65	35	1.0	60
70	40	1.25	75
75	45	1.5	90
80	50	1.75	105
85	55	2.0	120
90	60	-	135
95	65	-	150
-	70	-	165
-	75	-	180

Table 5.3: Plaque parameter relations. When varying the parameter in the left column according to table 5.2, the others were held constant as presented in each corresponding row.

Variable	Plaque circumference (%)	Lumen size (%)	NC thickness (mm)	NC angle (°)
Plaque circumference	-	30	0.5	60
Lumen size	75	-	0.5	60
NC thickness	75	50	-	60
NC angle	75	50	1.5	-

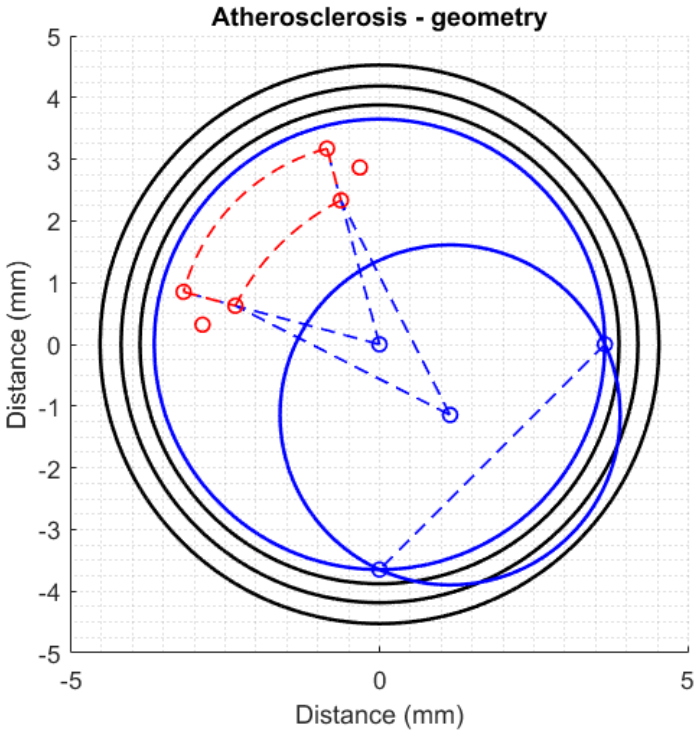

Figure 5.1: Example of artery geometry. The moon shaped plaque is outlined with blue borders and the necrotic core is represented by the red dotted line (with ends in the form of half circles).

5.2 Simulations

The physical behaviour of an artery afflicted by atherosclerosis was to be simulated using Abaqus/CAE, version 6.14-5. The geometries were drawn in Abaqus, following the blueprints described in section 5.1. The *Holzapfel-Gasser-Ogden* material model (see section 4.1) was used to describe the artery segments as well as the plaque excluding the necrotic core. The necrotic core on the other hand was modelled with a *neo-Hookean* model (section 4.2). All parameters used in the two models can be seen in table 5.4.

The artery wall segments were aligned with cylindrical coordinates to the origin of the original, atherosclerosis-free lumen, while the plaque was oriented to the new lumen origin. Meshing was done using 3-node, 2-D linear plane strain elements, with element sizes chosen in a trade-off between simulation speed and results. An example of an artery drawn in Abaqus together with the meshed version is shown in figure 5.2 An

Table 5.4: Material model parameters for the different segments of the artery and atherosclerotic plaque. c denotes the neo-Hookean parameter, D is associated with the material's compressibility, k_1 is related to stress and k_2 is dimensionless. κ is a parameter representing the fibre distribution in the HGO model. Parameters from [9][20] (c, k_1, k_2), [2] (κ) and [19] (D).

	c (kPa)	D (Pa^{-1})	k_1 (kPa)	k_2	κ
Adventitia	$7.56{\cdot}10^3$	$4.67{\cdot}10^{-6}$	$19.29{\cdot}10^3$	85.03	0.097
Media	$27.9{\cdot}10^3$	$0.895{\cdot}10^{-6}$	$131.83{\cdot}10^3$	170.88	0.095
Intima	$1.27{\cdot}10^3$	$5.31{\cdot}10^{-6}$	$10.8{\cdot}10^3$	8.21	0.2
Necrotic core	$5{\cdot}10^3$	$10{\cdot}10^{-6}$	-	-	-

Abaqus parameter called "global seeds", which controls the size of the elements and depends on the size of the meshed object, was set to 0.0001. The different segments were held together by adding a tie constraint, where the plaque border connected to the intima was chosen to be the master surface. Spatial constraints were set on the outer boundary of the artery wall, with zero possibility of movement in any direction for the outermost nodes.

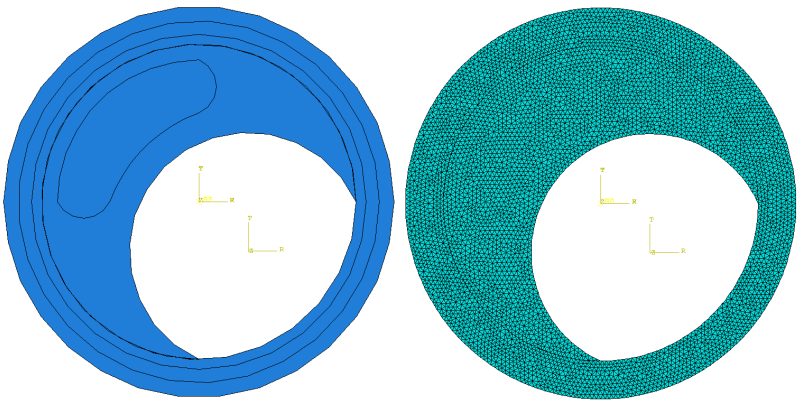

Figure 5.2: Example of artery with mesh drawn in Abaqus. The artery wall segments are aligned to the original lumen origin and the plaque is oriented to the new lumen origin.

The blood pressure was simulated not as absolute values but as a regular resting difference between systole and diastole. A two-step pressure load was therefore applied on the lumen boundaries, adding first an internal pressure of 80 mmHg (10.666 kPa) and then increasing it to 120 mmHg (16 kPa). After completing the simulation, the difference of

stresses induced between the two steps were studied while keeping the spatial effects from the second step. A stress map covering the Tresca stress throughout the artery was saved along with data of Tresca and circumferential stresses on the plaque-lumen boundary.

This simulation was repeated for all different geometries (see tables 5.2 and 5.3). The results were compiled and studied with regards to the variable geometry parameters.

6 Results

Stress maps of the atherosclerotic plaques resulting from the simulations are presented in figures 6.1-6.4. Maximum circumferential and Tresca stress measured on the border between plaque and lumen can be seen in figure 6.5. Typical stress plots on the plaque-lumen boundary are shown in figure 6.6.

Figure 6.1 shows what happens when the plaque circumference is varied from 55 % to 95 %, and indicates higher Tresca stress values close to the necrotic core as the ratio increases. This is also visible in the first row of figure 6.5, where the maximum detected stresses are trending upwards as the plaque surrounds more and more of the intima. The distribution of stress throughout the plaque is also increasingly diversified, with areas by the lumen and close to the edges of the necrotic core having higher stress values.

The results from varying the lumen coverage can be seen in figure 6.2. The spread in stress values is greater than for the circumference results (compare legends), but the spread is primarily in the radial direction (from the perspective of the new lumen origin). Stress values on the lumen border are increased with narrowing of the lumen (see also second row of figure 6.5), while the impact on the rest of the plaque is dampened with lower stress values as a result.

The effect of increasing the thickness of the necrotic core is visible in figure 6.3. With a thin core (and therefore thick cap) the Tresca stresses are relatively low and evenly distributed in the circumferential direction. However, as the cap thickness becomes smaller the stress maps show more discrepancies, with the highest stress values in the region between the necrotic core and the lumen. Figure 6.5 (third row) shows large increases of maximum stress values (for both circumferential and Tresca stresses) as the cap gets smaller.

The results from varying the the last parameter studied in the report, the angle of the necrotic core, are presented in figure 6.4. The minimum and maximum Tresca stress values in each instance are similar, but the difference in the distribution is large. With a small angle the largest stresses are found on the part of the lumen border closest to the edges of the necrotic core. This continues to be true when the angle is large, but the same level of stresses is then visible between these points as well. In the last row of figure 6.5, the two plots show a slight increase of the maximum circumferential and Tresca stresses.

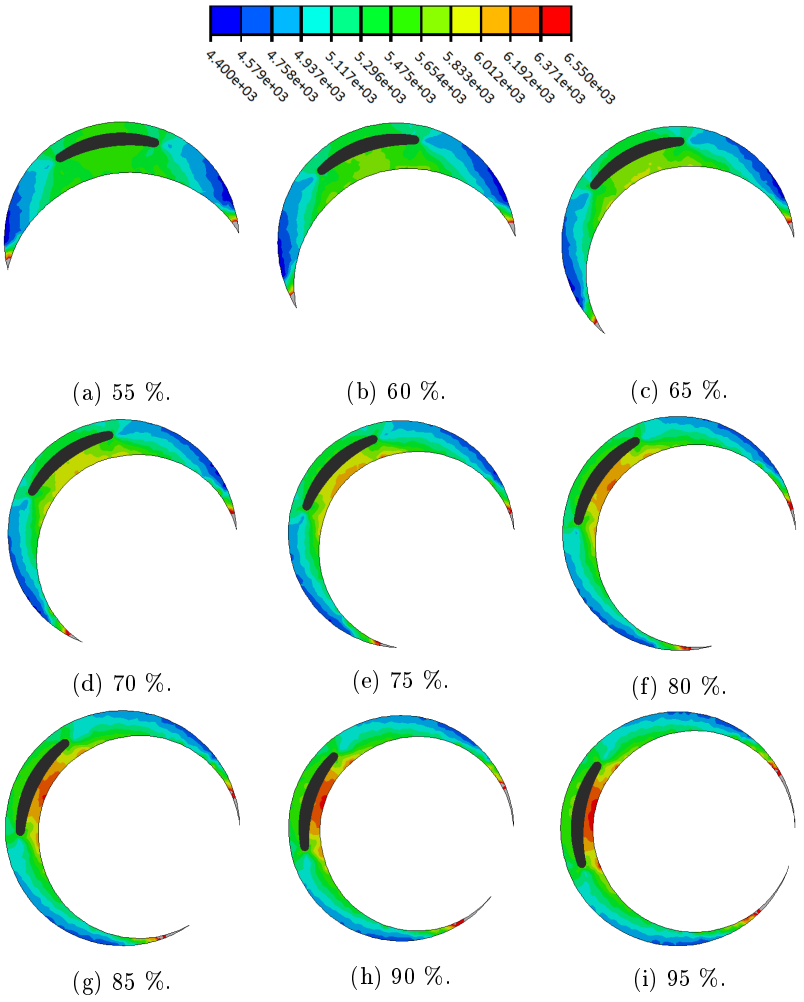

(a) 55 %. (b) 60 %. (c) 65 %.

(d) 70 %. (e) 75 %. (f) 80 %.

(g) 85 %. (h) 90 %. (i) 95 %.

Figure 6.1: Tresca stress maps over the atherosclerotic plaque with the plaque circumference ranging from 55 % to 95 %. Legend in Pa. Lumen coverage, NC thickness and angle are held constant at 30 %, 0.5 mm and 60°.

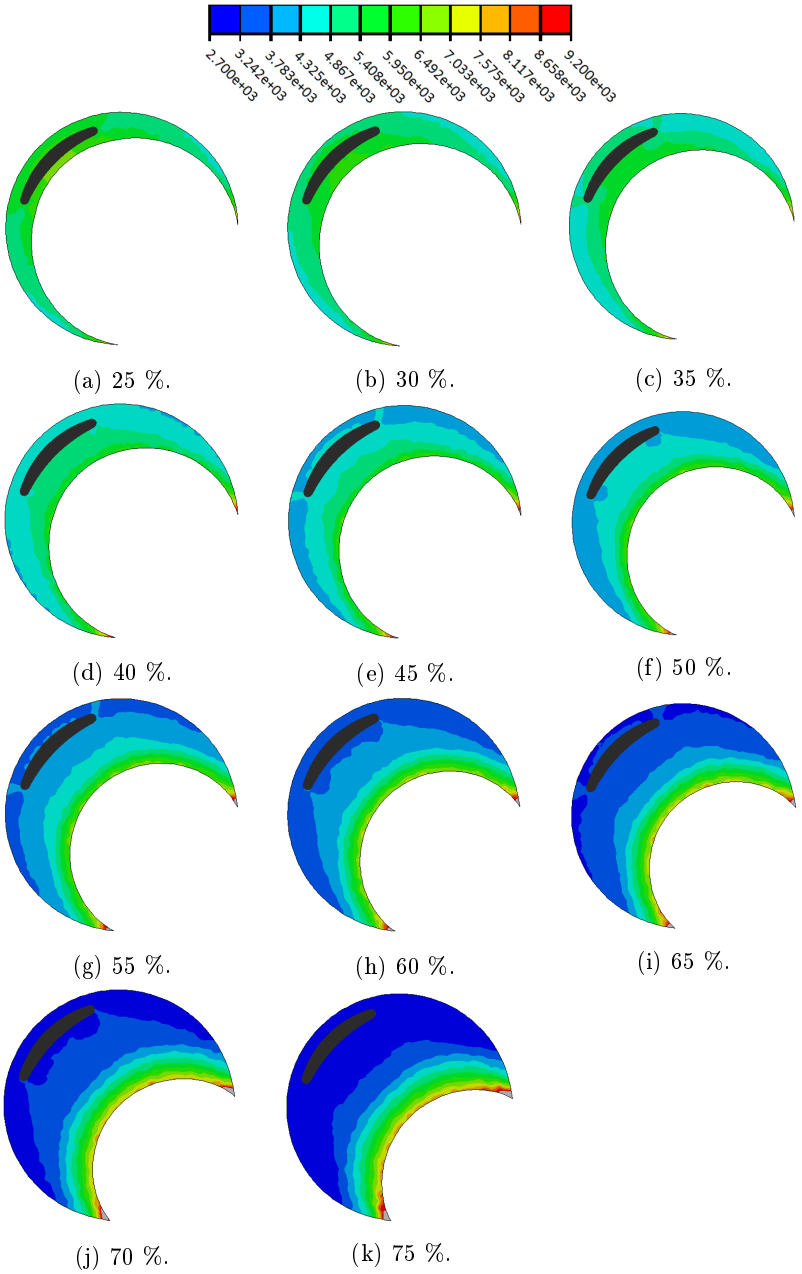

(a) 25 %. (b) 30 %. (c) 35 %.

(d) 40 %. (e) 45 %. (f) 50 %.

(g) 55 %. (h) 60 %. (i) 65 %.

(j) 70 %. (k) 75 %.

Figure 6.2: Tresca stress maps over the atherosclerotic plaque with the lumen coverage ranging from 25 % to 75 %. Legend in Pa. Plaque circumference, NC thickness and angle are held constant at 75 %, 0.5 mm and 60°.

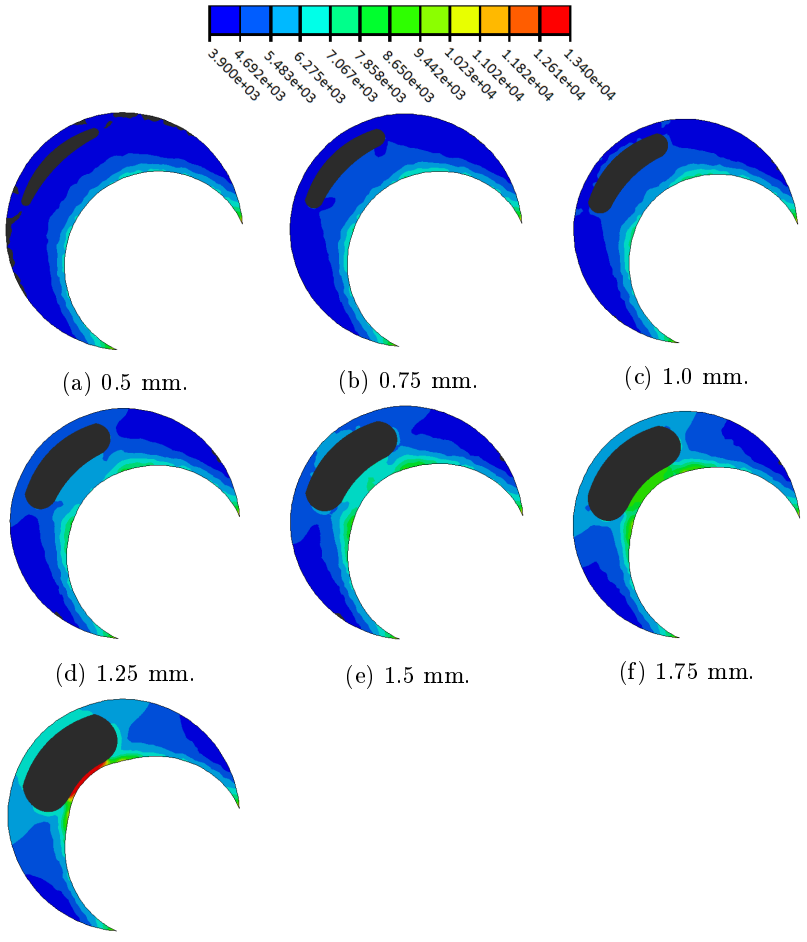

(a) 0.5 mm. (b) 0.75 mm. (c) 1.0 mm.

(d) 1.25 mm. (e) 1.5 mm. (f) 1.75 mm.

(g) 2.0 mm.

Figure 6.3: Tresca stress maps over the atherosclerotic plaque with the necrotic core thickness ranging from 0.5 mm to 2.0 mm. Legend in Pa. Plaque circumference, lumen coverage and NC angle are held constant at 75 %, 50 % mm and 60°.

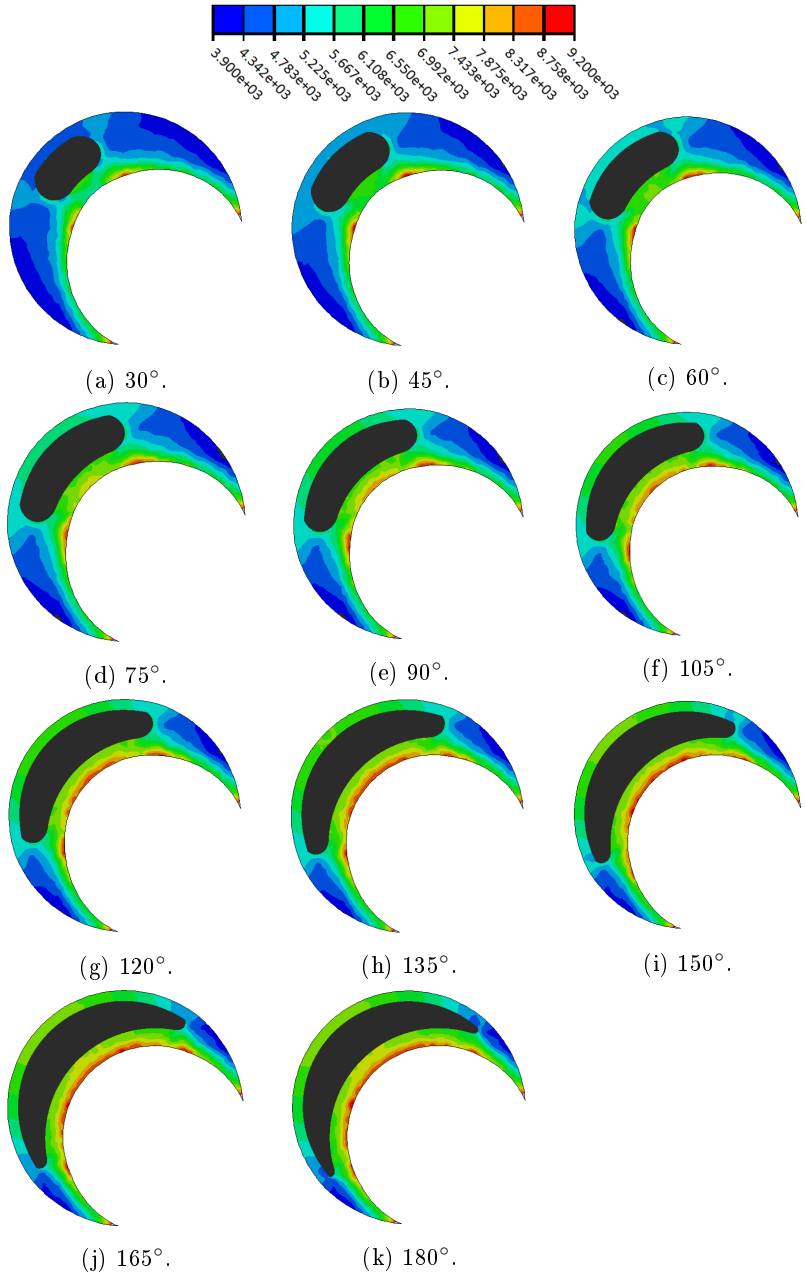

(a) 30°. (b) 45°. (c) 60°.

(d) 75°. (e) 90°. (f) 105°.

(g) 120°. (h) 135°. (i) 150°.

(j) 165°. (k) 180°.

Figure 6.4: Tresca stress maps over the atherosclerotic plaque with the necrotic core angle ranging from 30° to 180°. Legend in Pa. Plaque circumference, lumen coverage and NC thickness are held constant at 75 %, 50 % and 1.5 mm.

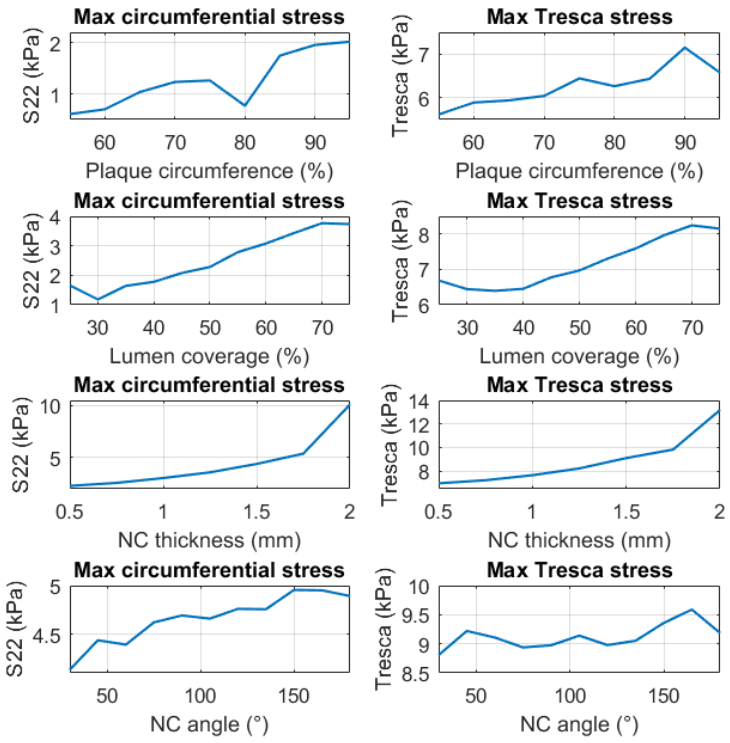

Figure 6.5: Maximum circumferential (S22, left column) and Tresca (right column) stress measured on the border between plaque and lumen in each simulation, plotted against the respective variable parameter. The outermost ends of the border has been neglected. The first row of plots is from the plaque circumference simulations, second from lumen coverage, third from NC thickness and fourth from the NC angle simulations.

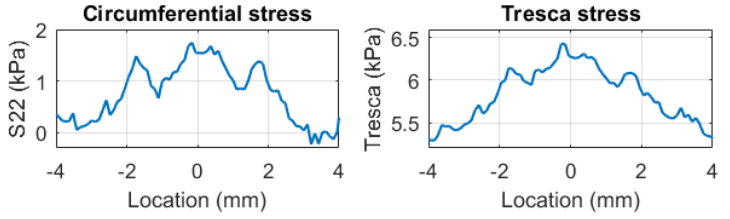

Figure 6.6: Typical stress plots on the plaque-lumen boundary. Plaque circumference is 85 %, lumen coverage is 30 %, NC thickness is 0.5 mm and NC angle is 60°. The outermost ends of the border has been neglected. The location is measured from the centre of the plaque-lumen boundary, i.e. "0 mm" is located in the middle between the two plaque edges.

7 | Discussion

The results from the simulations clearly indicates that the stability of an atherosclerotic lesion depends on the plaque distribution. Particularly the parameter governing the thickness of the necrotic core gave large variations in peak stresses in both the circumferential direction and in the case of Tresca stress (figure 6.5).

Apart from the obvious, the lumen coverage also affects the thickness of the fibrous cap. It is therefore interesting that the peak stresses actually increases as the lesion grows larger, since it also means that the cap becomes thicker. However, the stress increase is not too large compared to the results from the necrotic core thickness (compare rows 2 and 3 in figure 6.5), and the peak stress curves actually begins with a decrease in magnitude. This indicates that the impact of the cap thickness is large in the first simulation of the series and becomes less so as the coverage increases. The eccentricity of the plaque geometry is probably what causes the rise in stresses later in the series. The lumen, which in reality would preferentially be circular in its cross-section, becomes more oval- or lemon-shaped. The pressure acts normal to the surfaces, and as the coverage expands the difference between the normals of the plaque and artery becomes larger. This increases the stresses induced on the plaque-lumen border, especially close to the plaque edges.

When the plaque covers more of the arterial wall the peak stress increases, but the focus area remains the same. It is important to note that when this parameter, the plaque circumference, is altered it also affects the thickness of the fibrous cap, since the distance between the necrotic core and the arterial wall is set to be constant. The cap is rather thin and comparable to the first three simulation over lumen coverage and the last three simulations over necrotic core thickness (compare in figures 6.1, 6.2 and 6.3). The corresponding values in the peak stresses over plaque circumference and lumen coverage are of the same order, but in the NC thickness case they are larger (rows 1, 2 and 3 in figure 6.5). The plaque covering larger portions of the circumference seems therefore to have a dampening effect on the stresses rather than increasing them, and the increase in stresses visible in the results are due to the fibrous cap becoming thinner. It is the same concept as for the lumen coverage; the more eccentric the distribution the more stresses are induced in the structure. Because of the fact that the stresses increases it also shows that the impact of decreasing the cap thickness, even by the relatively small amount present in the series, is greater than increasing the circumferential coverage from 55 % to 95 %.

It is evident from the simulation series that the most influential component of the plaque on its own stability is the necrotic core. The peak

stress levels are lower in the first two series compared to the second two, most notable for the circumferential stresses but also in the Tresca case (figure 6.5). The peak stress NC thickness plots shows exponential properties, but in the NC angle case the results are much more diffuse (row 4 of figure 6.5). The stress increases are there but they are small and unsteady, particularly for the peak Tresca stresses. Studying the series in figure 6.4 it is clear that high levels of stress are present from the start of the series, when the angle is small. What is happening, however, is that the areas of high stresses expand and covers close to the whole of the plaque-lumen boundary when the angle is large. The stability of the lesion is therefore being compromised, since the overall stresses induced into the plaque are increasing.

The plaque edges are in all simulations subject to high stresses. These stress levels are mainly not physiological but are instead artefacts from the simulations. The number of elements radially constituting the plaque in these parts is low, often just one or two, which together with the difference in the load direction between the plaque and the intima gives rise to these high levels of stress. It is because of their origin that these results were excluded from the peak stress calculations as well as the plaque-lumen boundary stress plot (figure 6.6).

The load pressure was applied in two steps and the presented results are given by the difference in induced stresses between them. This idea came from the study described in section 3.2 where the initial stresses in the plaque are taken into account. *In-vivo*, an artery segment with or without lesion is always affected by blood pressure and in a stress-free environment it would contract considerably. Since the simulations would start with geometries close to the end result it was thought to be best to use this two-step difference approach. Each step on its own was thought to be further from actual stress values than the difference between them. However, it also means that comparisons with other studies are a bit harder to do.

The finite element study presented in section 3.2 ([20]) reported an average von Mises stress at the caps of 87±56 kPa with initial stress at 140 mmHg, and the study in section 3.3 ([17]) reported an average circumferential stress of 65.6±21.4 kPa at 100 mmHg. Compared to these values the magnitude of the results in this project are reasonable. However, the study in section 3.1 ([5]) reports considerably higher peak circumferential stresses, averaging at 545.4 kPa in ruptured plaques and 192.5± kPa in control lesions, at 110 mmHg. Comparing the material parameters in tables 3.1 and 3.2, which are both for transversely isotropic models, it is clear that the difference in applied load between the two studies is not the only possible cause for the difference in results. This highlights both the importance of proper material parameters as well as the diversity of plaque mechanical properties, since both reports studied specific lesions. Stress-strain relationship studies of different plaque

specimens in [12] show that the different results in [5], [20] and [17] are all possible, again due the plaque diversity. It should also be emphasised that the lesions examined in [20] and [17] were not necessarily unstable.

As mentioned, compared to stresses at 65.6 or even 87 kPa, the results from the simulations in this project are reasonable. Peak cap stress increases of ~ 10 kPa, as the case is for the necrotic core thickness series, are quite significant when these ranges are considered, while increases of one or two kPa might not contribute much in terms of plaque stability. However, the aim of the simulations in this report was not to produce the most precise levels of stresses in an atherosclerotic plaque. Instead, the idea was to study the general mechanical responses of lesions with different distributions. It should also be noted that patients with atherosclerosis often have higher blood pressure than the regular 120/80 mmHg, which if accounted for would have contributed to higher stresses in the simulations.

The Holzapfel-Gasser-Ogden model is central in this project. It is based on non-linear, anisotropic elasticity theory and accounts for fibre dispersion in a rather simple way, since it only requires one scalar structural parameter to be described. The main reason why this model was chosen was that it is able to capture the typical non-linear responses of arterial tissue and still be relatively simple. The model is also incorporated into Abaqus/CAE, which made it straightforward to perform the simulations. A more advanced model would perhaps not have improved this study that much, since the aim was give a better understanding of atherosclerotic plaques in general. Stability evaluations of specific, actual plaques would of course benefit much more from more advanced material models.

The parameters used for the different segments are not all together fitted to experimental data, which would have been the ideal case. In [9], mechanical tests are carried out on coronary arteries and the results are fitted to a model similar to the one used here. The same thing is done in [2] but with carotid arteries. Since the dispersion parameter κ is from this source, it is a clearly a possible source of error. Another source of uncertainty is the incompressibility parameter D. The model assumes incompressibility of the arteries, but Abaqus requires that enough compressibility is provided. The only source found containing values of D was [19], which is not as satisfactory as [9] or [2].

7.1 Future work

The methodology of the simulations carried out in this project can be improved. It would be interesting to study the effect of implementing initial stress into the procedure, since it would be a more realistic approach to the environment of the artery and plaque. More variations in the plaque distribution would also be of interest, with for instance

multiple cores or total coverage of the intima.

The parameters used in the models are an uncertainty. More experimental data on coronary arteries with atherosclerotic plaques could be used to give more reliable parameters. The general nature of this study is in many aspects a good thing, but it can also be extended to include different cases of plaque composition. This would, however, require even more experimental data.

8 | Conclusions

Atherosclerosis is a complex disease with many underlying factors to consider. ESS and inflammation are two key components which governs both the development of a plaque and its progression to an unstable lesion.

The finite element simulations carried out in this project showed that the structural parameters governing the atherosclerotic plaque's geometry influenced the stress distribution induced into the lesion. The most influential structural parameter considered was the thickness of the necrotic core, since it directly affects the thickness of the fibrous cap. Increases of all parameters considered gave higher maximum stress values at the plaque-lumen border, but with different magnitude and properties of the stress-parameter curves. When evaluating the stability of a plaque it is therefore of importance to consider the plaque's structural distribution.

9 | Appendix

9.1 Matlab geometry code

Complete Matlab code for the artery and plaque geometry construction.

```
% Parameters
n_c = 0.75;          % Plaque circumference coverage ratio
n_l = 0.50;          % Plaque/Orig lumen area ratio
nct = 1.0*10^-3;     % Necrotic core thickness
nca = 60*2*pi/360;   % Necrotic core angle

nc_r = 0.90;
% Necrotic core outer radius (percentage of lumen radius)
t = 10^5;            % Precision

disp(['Plaque circumference ratio: ' num2str(n_c)])
disp(['Lumen area coverage ratio:  ' num2str(n_l)])
disp(['Necrotic core angle:        '
  num2str(nca/(2*pi)*360) 'deg'])
disp(['Necrotic core thickness:    '
  num2str(nct*10^3) ' mm'])
disp(' ')

% Holzapfel's dimensions of layers
ro = 4.5*10^-3;                 % Outer wall thickness
wt = 0.189*ro;                  % Wall thickness
rl = ro - wt;                   % Radius lumen
it = 0.27*wt;                   % intima thickness
mt = 0.36*wt;                   % media thickness
at = 0.4*wt;                    % adventitia thickness
ri = rl + it;                   % Radius intima
rm = ri + mt;                   % Radius media
ra = rm + at;                   % Radius adventitia

disp(['Radius lumen:      ' num2str(rl*10^3) ' mm'])
disp(['Radius intima:     ' num2str(ri*10^3) ' mm'])
disp(['Radius media:      ' num2str(rm*10^3) ' mm'])
disp(['Radius adventitia: ' num2str(ra*10^3) ' mm'])
disp(' ')

% Points A and B, angle and distance between them
phi_AB = round(2*pi*(1 - n_c), 8);
```

```
xA = rl; yA = 0;

xB = round(rl*cos(-phi_AB), 8);
yB = round(rl*sin(-phi_AB), 8);
d_AB = sqrt((xA - xB)^2 + (yA - yB)^2);

% Line through C, i.e. perpendicular to the A-B line
x_mAB = (xA+xB)/2; y_mAB = (yA+yB)/2;
% Point inbetween A and B
d_mAB = sqrt(x_mAB^2 + y_mAB^2);
% Distance from it to origin
if x_mAB ~= 0 && xB ~= xA
kAB = (xA-xB)/(-yA+yB); mAB = y_mAB-kAB*x_mAB;
elseif x_mAB == 0
kAB = t*10^6; mAB = 0;
else
kAB = 0; mAB = 0;
end
xC_r = rl*cos(pi-phi_AB/2); yC_r = rl*sin(pi-phi_AB/2);

x_l = linspace(xC_r, x_mAB, t);
y_l = linspace(yC_r, y_mAB, t);

% Find point C
xC = 0; yC = 0;
% Point C
xp0 = 0; yp0 = 0; rp = 0;
% Origin and radius of the plaque
res = 1;
% residual
for k = 2:t-1
xC_t = x_l(k); yC_t = y_l(k);   % Point C test

% Line perpendicular to line between C and A
x_mAC = (xC_t + xA)/2; y_mAC = (yC_t + yA)/2;
kAC = (xA-xC_t)/(-yA+yC_t); mAC = y_mAC-kAC*x_mAC;

% Intersection - Plaque origin
xp0_t = (mAC - mAB)/(kAB - kAC);
yp0_t = kAB*xp0_t + mAB;
rp_t = sqrt((xp0_t - xA)^2 + (yp0_t - yA)^2);

% Lumen coverage - circle segments
A_a = pi*rl^2;
% Area artery
```

```
A_l = pi*rp_t^2;
% Area lumen (more or less)
A_sl = rl^2/2*(phi_AB - sin(phi_AB));
% Area of artery circle segment
phi_ABp = acos((2*rp_t^2 - d_AB^2)/(2*rp_t^2));
% Angle between A and B from plaque origin
A_sp = rp_t^2/2*(phi_ABp - sin(phi_ABp));
% Area of lumen circle segment

d_p0 = sqrt(xp0_t^2 + yp0_t^2);
% Distance from origin to plaque origin
if d_p0 < d_mAB
A_pla = A_a - A_l + A_sp - A_sl;
elseif d_p0 > d_mAB
A_pla = A_a - A_sp - A_sl;
else
A_pla = A_a - A_l/2 - A_sl;
end
A_r = A_pla/A_a;
err = abs(n_l - A_r);

if err < res
res = err;
xC = xC_t;
yC = yC_t;
xp0 = xp0_t; yp0 = yp0_t; rp = rp_t;
end
end

% Display results
disp(['xA: ' num2str(xA) ', yA: ' num2str(yA)]);
disp(['xB: ' num2str(xB) ', yB: ' num2str(yB)]);
disp(['xC: ' num2str(xC) ', yC: ' num2str(yC)]);
disp(['Residual: ' num2str(res)]); disp(' ')

% Necrotic core
rnc_o = rl*nc_r;
% Outer radius of nc
rnc_i = rnc_o + sqrt(xp0^2 + yp0^2) - nct;
% Inner radius of nc
phi_nc = pi - phi_AB/2;
% Angle between x-axis and the middle of the nc
phi_nc1 = phi_nc + nca/2;
% Angle between x-axis and the 1st corner (lower left)
phi_nc2 = phi_nc - nca/2;
```

```
% Angle between x-axis and the 2nd corner (upper right)
pth = rnc_i - rp;
% Plaque cap thickness
disp(['Plaque cap thickness: ' num2str(pth)]); disp(' ')

xp1_nc1 = rnc_o*cos(phi_nc1); yp1_nc1 = rnc_o*sin(phi_nc1);
% Nc point 1 corner 1
xp1_nc2 = rnc_o*cos(phi_nc2); yp1_nc2 = rnc_o*sin(phi_nc2);
% Nc point 1 corner 2
xl_nc1 = linspace(0, xp1_nc1, t);
yl_nc1 = linspace(0, yp1_nc1, t);
% Nc line from origin to corner 1
xl_nc2 = linspace(0, xp1_nc2, t);
yl_nc2 = linspace(0, yp1_nc2, t);
% Nc line from origin to corner 2

% Find inner nc circle boundaries
d_nc1 = abs(sqrt((xl_nc1 - xp0).^2 +
(yl_nc1 - yp0).^2) - rnc_i);
d_nc2 = abs(sqrt((xl_nc2 - xp0).^2 +
(yl_nc2 - yp0).^2) - rnc_i);
ind1 = find(d_nc1 == min(d_nc1));
ind2 = find(d_nc2 == min(d_nc2));
xp2_nc1 = xl_nc1(ind1); yp2_nc1 = yl_nc1(ind1);
% Nc point 2 corner 1
xp2_nc2 = xl_nc2(ind2); yp2_nc2 = yl_nc2(ind2);
% Nc point 2 corner 2

% Find nc end circles
x0_nc1 = (rnc_o*cos(phi_nc1) + xp2_nc1)/2;
y0_nc1 = (rnc_o*sin(phi_nc1) + yp2_nc1)/2;
r0_nc1 = sqrt((x0_nc1 - xp2_nc1)^2 + (y0_nc1 - yp2_nc1)^2);

x0_nc2 = (rnc_o*cos(phi_nc2) + xp2_nc2)/2;
y0_nc2 = (rnc_o*sin(phi_nc2) + yp2_nc2)/2;
r0_nc2 = sqrt((x0_nc2 - xp2_nc2)^2 + (y0_nc2 - yp2_nc2)^2);

phi0_nc1 = 3/2*pi - phi_nc1; phi0_nc2 = pi/2 - phi_nc2;
% Angles from nc corner origins to nc point 3
xp3_nc1 = x0_nc1 + r0_nc1*cos(-phi0_nc1);
% Nc point 3 corner 1
yp3_nc1 = y0_nc1 + r0_nc1*sin(-phi0_nc1);
xp3_nc2 = x0_nc2 + r0_nc2*cos(-phi0_nc2);
% Nc point 3 corner 2
yp3_nc2 = y0_nc2 + r0_nc2*sin(-phi0_nc2);
```

```
% Display results
disp('Corner 1')
disp(['x_p1: ' num2str(xp1_nc1) ', yp1: '
  num2str(yp1_nc1)]);
disp(['x_p2: ' num2str(xp2_nc1) ', yp2: '
  num2str(yp2_nc1)]);
disp(['x_p3: ' num2str(xp3_nc1) ', yp3: '
  num2str(yp3_nc1)]);
disp('Corner 2')
disp(['x_p1: ' num2str(xp1_nc2) ', yp1: '
  num2str(yp1_nc2)]);
disp(['x_p2: ' num2str(xp2_nc2) ', yp2: '
  num2str(yp2_nc2)]);
disp(['x_p3: ' num2str(xp3_nc2) ', yp3: '
  num2str(yp3_nc2)]);
disp(['xp0:  ' num2str(xp0) ',  yp0: ' num2str(yp0)])
disp(' ')
disp(['Plaque cap thickness: '
  num2str(pth*10^3) ' mm'])
disp(' ')

% Construct circles and plots
% Lumen
xl = linspace(-rl, rl, t);
yl1 = sqrt(rl^2-xl.^2); yl2 = -sqrt(rl^2-xl.^2);
% Plaque
xp = linspace(-rp, rp, t);
yp1 = sqrt(rp^2-xp.^2); yp2 = -sqrt(rp^2-xp.^2);
% Intima
xi = linspace(-ri, ri, t);
yi1 = sqrt(ri^2-xi.^2); yi2 = -sqrt(ri^2-xi.^2);
% Media
xm = linspace(-rm, rm, t);
ym1 = sqrt(rm^2-xm.^2); ym2 = -sqrt(rm^2-xm.^2);
% Adventitia
xa = linspace(-ra, ra, t);
ya1 = sqrt(ra^2-xa.^2); ya2 = -sqrt(ra^2-xa.^2);
% Inner necrotic core
phit1 = pi + atan((yp2_nc1 - yp0)/(xp2_nc1 - xp0));
phit2 = pi/2 + atan((xp0 - xp2_nc2)/(yp2_nc2 - yp0));
phi_nci = linspace(phit2, phit1, t);
xi_nc = rnc_i*cos(phi_nci) + xp0;
yi_nc = rnc_i*sin(phi_nci) + yp0;
% Outer necrotic core
```

```
phi_nco = linspace(phi_nc2, phi_nc1, t);
xo_nc = rnc_o*cos(phi_nco); yo_nc = rnc_o*sin(phi_nco);

% Figures
figure(2); hold on
title('Atherosclerosis - geometry')
xlabel('Distance (m)')
ylabel('Distance (m)')
axis equal;
axis([-5 5 -5 5].*10^-3)
grid minor

% Layers
plot(xl, yl1, 'b', 'LineWidth', 1.5)    % Lumen
plot(xl, yl2, 'b', 'LineWidth', 1.5)
plot(xi, yi1, 'black', 'LineWidth', 1.5)    % Intima
plot(xi, yi2, 'black', 'LineWidth', 1.5)
plot(xm, ym1, 'black', 'LineWidth', 1.5)    % Media
plot(xm, ym2, 'black', 'LineWidth', 1.5)
plot(xa, ya1, 'black', 'LineWidth', 1.5)    % Adventitia
plot(xa, ya2, 'black', 'LineWidth', 1.5)

% Plaque
plot(xp + xp0, yp1 + yp0, 'b', 'LineWidth', 1.5)
plot(xp + xp0, yp2 + yp0, 'b', 'LineWidth', 1.5)

% Necrotic core
plot(xl_nc1, yl_nc1, 'b--', 'LineWidth', 1)
% 1st line from origin to outer nc circle
plot(xl_nc2, yl_nc2, 'b--', 'LineWidth', 1)
% 2nd line from origin to outer nc circle
plot([xp0 xp2_nc1], [yp0 yp2_nc1], 'bo--', 'LineWidth', 1)
% 1st line from origin to inner nc circle
plot([xp0 xp2_nc2], [yp0 yp2_nc2], 'bo--', 'LineWidth', 1)
% 2nd line from origin to inner nc circle
plot([xp1_nc1 xp2_nc1], [yp1_nc1 yp2_nc1], 'ro--', 'LineWidth', 1)
plot([xp1_nc2 xp2_nc2], [yp1_nc2 yp2_nc2], 'ro--', 'LineWidth', 1)
plot(xp3_nc1, yp3_nc1, 'ro', 'LineWidth', 1)
plot(xp3_nc2, yp3_nc2, 'ro', 'LineWidth', 1)
plot(xi_nc, yi_nc, 'r--', 'LineWidth', 1)
plot(xo_nc, yo_nc, 'r--', 'LineWidth', 1)

% Lines and points
plot(0, 0, 'ob', 'LineWidth', 1)
% Origin
```

```
plot(xp0, yp0, 'ob', 'LineWidth', 1)
% Plaque origin
plot([xA xB], [yA yB], 'bo--', 'LineWidth', 1)
% Line between A and B
%     plot(x_l, y_l, 'g', 'LineWidth', 1)
% Line through origin

% Necrotic core rotation (from x-axis)
disp(['Rotation angle (from x-axis): '
  num2str(phi_nc*360/2/pi) 'deg'])
```

9.2 Abaqus input file

Input file example from a simulation. Information regarding nodes and elements have been removed due to the amount of space it would cover.

```
*Heading
** Job name: Job-85-30-5-60 Model name: Model-1
** Generated by: Abaqus/CAE 6.14-5
*Preprint, echo=NO, model=NO, history=NO, contact=NO
**
** PARTS
**
*Part, name=ArteryWall
*----------------------*
*Element, type=CPEG3
*----------------------*
*Orientation, name=Ori-1, system=CYLINDRICAL
0.,           0.,           0.,           0.,
0.,           1.
3, 0.
** Section: Media_sec
*Solid Section, elset=Set-2, orientation=Ori-1,
material=Media_mat, ref node=ArteryWall-RefPt_
1.,
** Section: Intima_sec
*Solid Section, elset=Set-3, orientation=Ori-1,
material=Intima_mat, ref node=ArteryWall-RefPt_
1.,
** Section: Adventitia_sec
*Solid Section, elset=Set-1, orientation=Ori-1,
material=Adventitia_mat, ref node=ArteryWall-RefPt_
1.,
*End Part
**
```

```
*Part, name=Plaque
*Node
*----------------------*
*Element, type=CPEG3
*----------------------*
*Orientation, name=Ori-1, system=CYLINDRICAL
0.000601,    -0.000306,           0.,     0.000601,
-0.000306,           1.
3, 0.
** Section: Intima_sec
*Solid Section, elset=Set-1, orientation=Ori-1,
material=Intima_mat, ref node=Plaque-RefPt_
1.,
** Section: NecroticCore_sec
*Solid Section, elset=Set-2, material=NecroticCore_mat,
ref node=Plaque-RefPt_
1.,
*End Part
**
**
** ASSEMBLY
**
*Assembly, name=Assembly
**
*Instance, name=ArteryWall-1, part=ArteryWall
*End Instance
**
*Instance, name=Plaque-1, part=Plaque
*End Instance
**
** Constraint: Constraint-1
*Tie, name=Constraint-1, adjust=yes
s_Set-1_CNS_, m_Surf-1
*End Assembly
**
** MATERIALS
**
*Material, name=Adventitia_mat
*Anisotropic Hyperelastic, holzapfel, local direction=1
7560., 4.67e-06,   19290.,    85.03,    0.097
*Material, name=Intima_mat
*Anisotropic Hyperelastic, holzapfel, local direction=1
27900., 8.95e-07,  131830.,   170.88,    0.095
*Material, name=Media_mat
*Anisotropic Hyperelastic, holzapfel, local direction=1
```

```
1270., 5.31e-06,   10800.,     8.21,      0.2
*Material, name=NecroticCore_mat
*Hyperelastic, neo hooke
5000., 1e-05
**
** BOUNDARY CONDITIONS
**
** Name: BC-1 Type: Displacement/Rotation
*Boundary
Set-2, 1, 1
Set-2, 2, 2
** ----------------------------------------
**
** STEP: ApplyPressure1
**
*Step, name=ApplyPressure1, nlgeom=YES
*Static
1., 1., 1e-05, 1.
**
** LOADS
**
** Name: Pressure1   Type: Pressure
*Dsload
Surf-2, P, 10666.
** Name: Pressure2   Type: Pressure
*Dsload
Surf-3, P, 10666.
** Name: Pressure3   Type: Pressure
*Dsload
Surf-4, P, 10666.
**
** OUTPUT REQUESTS
**
*Restart, write, frequency=0
**
** FIELD OUTPUT: F-Output-1
**
*Output, field, variable=PRESELECT
**
** HISTORY OUTPUT: H-Output-1
**
*Output, history, variable=PRESELECT
*End Step
** ----------------------------------------
**
```

```
** STEP: ApplyPressure2
**
*Step, name=ApplyPressure2, nlgeom=YES
*Static
1., 1., 1e-05, 1.
**
** LOADS
**
** Name: Pressure1   Type: Pressure
*Dsload
Surf-2, P, 16000.
** Name: Pressure2   Type: Pressure
*Dsload
Surf-3, P, 16000.
** Name: Pressure3   Type: Pressure
*Dsload
Surf-4, P, 16000.
**
** OUTPUT REQUESTS
**
*Restart, write, frequency=0
**
** FIELD OUTPUT: F-Output-1
**
*Output, field, variable=PRESELECT
**
** HISTORY OUTPUT: H-Output-1
**
*Output, history, variable=PRESELECT
*End Step
```

Glossary

apoptosis Process of programmed cell death. In contrast to necrosis (form of traumatic cell death), apoptosis is a highly regulated and controlled process. 6

arteriosclerosis Thickening, hardening and loss of elasticity of the artery wall. 4

atheroma Accumulation of degenerative material in the tunica intima of artery walls. The material consists of cells, lipids, connective tissue and debris from the blood. 7

atherosclerosis Specific form of arteriosclerosis in which an artery wall thickens as a result of the formation of atheroma. 1, 2, 4, 5, 8, 17, 30

endothelium Type of epithelium that lines the interior surface of blood vessels and lymphatic vessels, forming an interface between circulating blood or lymph in the lumen and the rest of the vessel wall. 3–6

epithelium One of the four main types of animal tissue (the others being connective tissue, muscle tissue and nervous tissue). Epithelial tissues line the cavities and surfaces of blood vessels and organs throughout the body. 41

extracellular matrix Collection of extracellular molecules secreted (produced and discharged) by cells that provide structural and biochemical support to the surrounding cells. 1, 4

fibrous cap Layer of fibrous connective tissue, which is thicker and less cellular than the normal intima, found in atherosclerotic plaques. It contains macrophages and smooth muscle cells, foam cells, lymphocytes, collagen and elastin. 7, 9, 26, 30

hemodynamic Of or relating to the flow of blood within organs and tissues of the body. 1, 5

hypercholesterolemia Form of dyslipidemia, i.e. abnormal amounts of lipids (in this case cholesterol) in the blood. 5

hyperplasia Increase of number of cells. i, 4, 5

hypertension Also known as high blood pressure. Long term medical condition in which the blood pressure in the arteries is persistently elevated. 5

hypertrophy Increase of cell size. 4

ischemia Restriction of blood supply to tissues, causing shortages of oxygen and glucose needed for cellular metabolism. 1

leukocyte White blood cell. Part of the immune system involved in protecting the body against both infectious diseases and foreign invaders. 3, 4, 6

lipoprotein A biochemical assembly with the purpose of transporting hydrophobic lipid molecules in water, as for instance in blood. 3, 4

lumen The inside of a tubular structure, such as an artery or intestine. 3, 7, 9, 10, 15, 17–20, 22–27, 30

macrophage Type of white blood cells that engulfs and digests cellular debris, foreign substances, microbes, cancer cells and anything else that doesn't have the types of proteins specific for healthy body cells on it's surface in a process called phagocytosis. 1, 6, 7

monocyte Type of white blood cell (leukocyte). They are the largest type of leukocyte and can differentiate into macrophages. 6

platelet Disk-like cytoplasmic formation that promotes blood clotting. Also called thrombycyte. 3, 5

stenosis Narrowing of blood vessel or other tubular organ or structure. i, 1, 10

tensor invariant Invariants of a tensor are coefficients of the characteristic polynomial of the tensor. The first invariant is the coefficient for λ^{n-1} (since the coefficients for λ^n is always 1), the second invariant is the coefficients for λ^{n-2}, and so on. 13

thrombosis Formation of a blood clot inside a blood vessel, obstructing the blood flow through the circulatory system. The body uses platelets (thrombocytes) and fibrin to form a blood clot to prevent blood loss in damaged blood vessels. A clot that breaks free and travels through the body is called an embolus. 42

thrombus Blood clot. Consists of platelets, red blood cells and a mesh of fibrin protein. May be a healthy response to injury or harmful in thrombosis, where blood flow is obstructed due to the presence of the clot. 5, 6

Bibliography

[1] Abaqus Inc. Abaqus analysis user's guide, 6.14. `http://129.97.46.200:2080/v6.14/books/usb/default.htm`. [Accessed 06-March-2017].

[2] D. Balzani, S. Brinkhues, and G. A. Holzapfel. Constitutive framework for the modeling of damage in collagenous soft tissues with application to arterial walls. *Comput. Methods Appl. Mech. Engrg.*, (213-216):139–151, 2012.

[3] Blausen.com staff. Medical gallery of blausen medical. WikiJournal of Medicine, `https://commons.wikimedia.org/wiki/File:Blausen_0055_ArteryWallStructure.png`, 2014. [Accessed 2017-03-08].

[4] Y. S. Chatzizisis et al. Role of endothelial shear stress in the natural history of coronary atherosclerosis and vascular remodeling. *Journal of the American College of Cardiology*, 49(25), 2007.

[5] G. C. Cheng et al. Distribution of circumferential stress in ruptured and stable atherosclerotic lesions. *Circulation*, (87):1179–1187.

[6] M. J. Davies. Stability and instability: Two faces of coronary atherosclerosis. *Circulation*, (94):2013–2020.

[7] T. C. Gasser, R. W. Ogden, and G. A. Holzapfel. Hyperelastic modelling of arterial layers with distributed collagen fibre orientations. *J. R. Soc. Interface*, 3(6), 2006.

[8] G. K. Hansson. Inflammation, atherosclerosis, and coronary artery disease. *The New England Journal of Medicine*, 352(16), 2005.

[9] G. A. Holzapfel et al. Determination of layer-specific mechanical properties of human coronary arteries with nonatherosclerotic intimal thickening and related constitutive modeling. *Am J Physiol Heart Circ Physiol*, (289):H2048–H2058, 2005.

[10] G. A. Holzapfel and T. C. Gasser. A viscoelastic model for fiber-reinforced composites at finite strains: Continuum basis, computational aspects and applications. *Computer Methods in Applied Mechanics and Engineering*, 190.

[11] G. A. Holzapfel and T. C. Gasser. A new constitutive framework for arterial wall mechanics and a comparative study of material models. *Journal of Elasticity*, (61):1–48, 2000.

[12] C. Lendon et al. Testing of small connective tissue specimens for the determination of the mechanical behaviour of atherosclerotic plaques. *Journal of Biomedical Engineering*, 15, 1993.

[13] M. X. Li et al. Numerical analysis of pulsatile blood flow and vessel wall mechanics in different degrees of stenoses. *Journal of biomechanics*, (40):3715–3724, 2007.

[14] P. Libby, P. M. Ridker, and A. Maseri. Inflammation and atherosclerosis. *Circulation*, (105):1135–1143, 2002.

[15] W. W. Nichols and M. O'Rourke. *McDonald's Blood Flow in Arteries*. Oxford University Press Inc., fifth edition, 2005.

[16] R. W. Ogden. *Non-Linear Elastic Deformations*. Dover Publications, Inc., dover edition, 1997.

[17] J. Ohayon et al. A three-dimensional finite element analysis of stress distribution in a coronary atherosclerotic plaque: *In-vivo* prediction of plaque rupture location. *Biomechanics Applied to Computer Assisted Surgery*, pages 225–241.

[18] R. Ross. Atherosclerosis - an inflammatory disease. *The New England Journal of Medicine*, 340.

[19] A. Schiavone and L. G. Zhao. A study of balloon type, system constraint and artery constitutive model used in finite element simulation of stent deployment. *Mechanics of Advanced Materials and Modern Processes*, 1(1), 2015.

[20] L. Speelman et al. Initial stress in biomechanical models of atherosclerotic plaques. *Journal of Biomechanics*, (44):2376–2682.

[21] P. H. Stone et al. Effect of the local hemodynamic environment on the de novo development and progression of eccentric coronary atherosclerosis in humans: Insights from prediction. *Elsevier*, 240(1), 2015.

[22] The Editors of Encyclopædia Britannica. Atherosclerosis. Encyclopædia Britannica, inc, `https://global.britannica.com/science/atherosclerosis`, 2007. [Accessed 2017-03-08].

[23] J. J. Wentzel et al. Endothelial shear stress in the evolution of coronary atherosclerotic plaque and vascular remodelling: current understanding and remaining questions. *Cardiovascular Research*, (96):234–243, 2012.

[24] L. Wexler et al. Coronary artery calcification: Pathophysiology, epidemiology, imaging methods, and clinical implications. *Circulation*, 94(5):1175–1192, 1996.

[25] World Health Organization. Cardiovascular diseases (CVDs). http://www.who.int/mediacentre/factsheets/fs317/en/, 2016. [Accessed 2017-01-31].